Inorganic Chemistry

Article

pubs.acs.org/IC

Lanthanide Complexes of Macrocyclic Polyoxovanadates by VO_4 Units: Synthesis, Characterization, and Structure Elucidation by X-ray Crystallography and EXAFS Spectroscopy

Masaki Nishio,[†] Shinnosuke Inami,[†] Misaki Katayama,[‡] Kazuhiko Ozutsumi,[‡] and Yoshihito Hayashi*[,†]

[†]Department of Chemistry, Graduate School of Natural Science and Technology, Kanazawa University, Kakuma, Kanazawa 920-1192, Japan

[‡]Department of Applied Chemistry, College of Life Sciences, Ritsumeikan University, Kusatsu, Shiga 525-8577, Japan

Supporting Information

ABSTRACT: Reactions of a tetravanadate anion, $[V_4O_{12}]^{4-}$, with a series of lanthanide(III) salts yield three types of lanthanide complexes of macrocyclic polyoxovanadates: $(Et_4N)_6[Ln^{III}V_9O_{27}]$ [Ln = Nd (**1**), Sm (**2**), Eu (**3**), Gd (**4**), Tb (**5**), Dy (**6**)], $(Et_4N)_5[(H_2O)Ho^{III}(V_4O_{12})_2]$ (**7**), and $(Et_4N)_7[Ln^{III}V_{10}O_{30}]$ [Ln = Er (**8**), Tm (**9**), Yb (**10**), Lu (**11**)]. Lanthanide complexes **1**−**11** are isolated and characterized by IR, elemental analysis, single-crystal X-ray diffraction, and extended X-ray absorption fine structure spectroscopy (EXAFS). Lanthanide complexes **1**−**6** are composed of a square-antiprism eight-coordinated Ln^{III} center with a macrocyclic polyoxovanadate that is constructed from nine VO_4 tetrahedra through vertex sharing. The structure of **7** is composed of a seven-coordinated Ho^{III} center, which exhibits a capped trigonal-prism coordination environment by the sandwiching of two cyclic tetravanadates with a capping H_2O ligand. Lanthanide complexes **8**−**11** have a six-coordinated Ln^{III} center with a 10-membered vanadate ligand. The structural trend to adopt a larger coordination number for a larger lanthanide ion among the three types of structures is accompanied by a change in the vanadate ring sizes. These lanthanide complexes are examined by EXAFS spectroscopies on lanthanide L_{III} absorption edges, and the EXAFS oscillations of each of the samples in the solid state and in acetonitrile are identical. The Ln−O and Ln···V bond lengths obtained from fits of the EXAFS data are consistent with the data from the single-crystal X-ray studies, reflecting retention of the structures in acetonitrile.

INTRODUCTION

Polyoxometalates possess remarkable structural diversity and exhibit various properties in a wealth of applications in fields such as photochemistry, clinical chemistry, magnetism, electric device, catalysis, and material science.[1] By the introduction of a heteroatom to a polyoxometalate framework, further diversification can be achieved and the resulting heteropolyoxometalates exhibit a wide range of catalytic applications.[2] Cyclic polyoxometalates such as Preyssler complexes[3] are especially interesting because of their ability to incorporate a heteroatom at the center of the ring, and the cavity is large enough to accommodate a lanthanide ion.[4,5] Lanthanide-incorporated heteropolyoxometalates elicit much interest because of their photoluminescence properties and catalytic abilities.[6] Typical heteropolyoxometalates such as Keggin- or Dawson-type compounds contain smaller heteroatoms in their tetrahedral cavities. Such heteroatoms include P^V, As^V, and Si^{IV}, and a 3d transition element may also be incorporated.[7] Lanthanide ions, however, are too large to be fully incorporated as heteroatoms into the tetrahedral cavity. Instead of sitting in the cavity, the higher-coordination-number lanthanide cations occupy a lacunary position in the parent structure and act as linker units to form a dimeric structure, such as a lanthanide-sandwiched decatungstate,[8] or to expand into a larger structure, as seen in $[As^{III}_{12}Ce^{III}_{16}(H_2O)_{36}W_{148}O_{524}]^{76-}$.[9] Unlike molybdate or tungstate chemistry, limited numbers of heteropolyoxovanadates are known, and they include $[PV_{14}O_{42}]^{9-}$,[10] $[Mn_2V_{22}O_{64}]^{10-}$, $[Mn_3V_{12}O_{40}H_3]^{5-}$,[11] and $[MV_{13}O_{38}]^{7-}$ (M = Mn, Ni).[12] The incorporation of Te^{6+} in the decavanadate frameworks has been reported, and the Mo-substituted complex $[H_2MoV_9O_{28}]^{3-}$ is synthesized as a mixture of positional isomers of the substituted species.[13] A disorder-free decavanadate derivative was recently reported in a mono-Pt^{IV}-substituted complex, $[H_2Pt^{IV}V_9O_{28}]^{5-}$.[14] The larger lanthanide ions are difficult to fit in the vanadate frameworks because of the smaller ionic radii of vanadium atoms, and the effort to incorporate lanthanide ions produces two- and three-dimensional materials where lanthanide ions act as bridging units.[15] In the course of our synthetic studies to grow polyoxovanadates from smaller units to larger units, we developed a synthetic method to incorporate heteroatoms in polyoxovanadates.[16] We found a metavanadate-based macrocyclic ligand that can bind a heteroatom at the center of the ring to form an all-inorganic complex. The ligand formation starts with tetravanadate $[V_4O_{12}]^{4-}$, which is too small to incorporate a metal cation at the center of the ring yet has excellent coordinating ability and forms supported complexes with organometallic cations[17] or coordination compounds.[18] There are several different sizes of cyclic metavanadates. Ring sizes larger than a pentamer, $[V_5O_{15}]^{5-}$, are unknown, but the size of the ring may be expanded by the addition of a heterometal cation in the metavanadate solution. The first example of such a macrocyclic complex may have been a reduced decavanadate, $[V_{10}O_{26}]^{4-}$.[19] It is not recognized as a heteropolyoxovanadate

Received: March 29, 2011
Published: December 23, 2011

dx.doi.org/10.1021/ic200638f | Inorg. Chem. 2012, 51, 784−793

complex because all of its metal atoms are vanadium atoms. A new look at this complex, $[(V^{IV}O)_2V^{V}{}_8O_{24}]^{4-}$, reveals that the macrocyclic $[VO_3]_8^{8-}$ ligand binds two vanadyl cations, $[V{=}O]^{2+}$, at the center of the molecule to form a divanadyl complex, which resembles a crown ether. In acetonitrile, the metavanadate species exists as an equilibrium mixture of tetravanadates that differ in their chain orientation, degree of protonation, and cyclization number. The addition of transition-metal salts induces an equilibrium shift toward the formation of larger cyclic polyoxovanadate species that can adjust to the size of the added metal cations.

Examples of inorganic macrocyclic polyoxovanadate complexes by VO_4 units include $[PdV_6O_{18}]^{4-}$, $[Cu_2V_8O_{24}]^{4-}$, and $[Ni_4V_{10}O_{30}(OH)_2(H_2O)_6]^{4-}$.[20] The ring sizes of these inorganic complexes correlate with the total charge on the heterometal units. Higher charges on the central unit correlate with larger cyclic polyoxovanadates, $[VO_3]_n^{n-}$. In other words, the positive charge of the cationic heterometal at the center compensates for the negative charge buildup of the larger polyoxovanadates $[VO_3]_n^{n-}$, which are large enough to incorporate metal cations within the ring. A similar metal-lacrown chemistry based on the aggregation of organic ligand complexes has been investigated.[21] In a reduced oxidation state of vanadium, cyclic heteropolyoxovanadium complexes, $[MV_6O_6\{(OCH_2CH_2)_2N(CH_2CH_2OH)\}_6]X$ (M = Li, Na, Mg, Mn, Fe, Co, Ni; X = Cl^-, Br^-), have been reported.[22] An Anderson-type crown-shaped polyoxovanadate with organic ligands, $[V_6O_{12}(OH)_3(O_2CCH_2CH_2NH_3)_3(SO_4)]^+$, can bind an anion at the center.[23]

The metavanadate-based macrocyclic ligand, $[VO_3]_n^{n-}$, can bind a single heteroatom at the center, and in some cases, it becomes large enough to allow the assembly of a binuclear or tetranuclear cluster unit within the ring. Two types of structurally interesting examples are known. One is the ferrocene-like $[Mn_2(V_5O_{15})_2]^{6-}$ with two cyclic pentavanadates sandwiching the edge-sharing octahedral dimanganese units, and the other is $[Co_2(OH_2)_2V_{10}O_{30}]^{6-}$ with a macrocyclic decavanadate supporting edge-sharing octahedra of Co^{II} centers.[24] Extended X-ray absorption fine structure spectroscopy (EXAFS) data of those complexes obtained in acetonitrile are consistent with the solid-state structures and show interesting chromism upon water exposure.

In this paper, we report the synthesis of novel lanthanide complexes of macrocyclic polyoxovanadates. The unique all-inorganic disk-shaped structures are examined by X-ray crystallography as well as EXAFS spectroscopy in the solid state and in an acetonitrile solution.

EXPERIMENTAL SECTION

Synthesis. All reagent-grade chemicals were purchased and used without further purification. Acetonitrile was distilled from P_2O_5 under a nitrogen atmosphere. The reagents, $(n\text{-}Bu_4N)_4[V_4O_{12}]$[25] and $(Et_4N)_4[V_4O_{12}]$,[26] were synthesized according to published procedures. All reactions and manipulations were carried out under a nitrogen atmosphere using Schlenk techniques or in a drybox.

*Preparation of $(Et_4N)_6[LnV_9O_{27}]$ [Ln = Nd^{III} (**1**), Sm^{III} (**2**), Eu^{III} (**3**), Gd^{III} (**4**)].* $(Et_4N)_4[V_4O_{12}]$ (240 mg, 1.05 mmol) was dissolved in acetonitrile (3 mL), and 0.1 mmol of anhydrous $LnCl_3$ ($NdCl_3$, 25.1 mg; $SmCl_3$, 25.7 mg; $EuCl_3$, 25.8 mg; $GdCl_3$, 26.4 mg) in acetonitrile (2 mL) was added. The suspension was stirred for a few days, and a pale-purple solution was obtained. The resulting solution was filtered and concentrated to 1 mL. Nearly colorless crystals were collected after 1 day. Yield: ca. 70 mg (ca. 40% based on Ln). Anal. Calcd for $(Et_4N)_6[NdV_9O_{27}]\cdot H_2O$: C, 31.43; H, 6.70; N, 4.58. Found: C, 31.33; H, 6.68; N, 4.60. Anal. Calcd for $(Et_4N)_6[SmV_9O_{27}]\cdot 4H_2O$: C, 30.43; H, 6.81; N, 4.44. Found: C, 30.48; H, 6.82; N, 4.37. Anal. Calcd for $(Et_4N)_6[EuV_9O_{27}]\cdot 7H_2O$: C, 29.56; H, 6.93; N, 4.31. Found: C, 29.44; H, 6.94; N, 4.31. Anal. Calcd for $(Et_4N)_6[GdV_9O_{27}]\cdot 2H_2O$: C, 30.91; H, 6.70; N, 4.51. Found: C, 30.80; H, 6.77; N, 4.55. IR (Nujol, 500−1000 cm^{-1}): **1**, 943(sh), 927(s), 896(s), 831(s), 798(sh), 782(s), 721(m), 665(s); **2**, 946(m), 925(m), 898(s), 833(m), 788(m), 721(w), 665(s), 653(s); **3**, 968(sh), 927(s), 898(s), 833(m), 792(m), 721(w), 665(s), 655(s); **4**, 948(m), 919(sh), 900(m), 835(m), 792(w), 721(s), 665(m).

*Preparation of $(Et_4N)_6[LnV_9O_{27}]$ [Ln = Tb^{III} (**5**), Dy^{III} (**6**)].* $(Et_4N)_4[V_4O_{12}]$ (240 mg, 1.05 mmol) was dissolved in acetonitrile (3 mL), and 0.095 mmol of anhydrous $LnCl_3$ ($TbCl_3$, 25.2 mg; $DyCl_3$, 25.5 mg) in acetonitrile (3 mL) was added dropwise. The solution was stirred overnight, and the resulting colorless solution was filtered and concentrated to 1 mL. Colorless crystals were collected after 1 day. Yield: ca. 70 mg (40% based on Ln). Anal. Calcd for $(Et_4N)_6[TbV_9O_{27}]\cdot 2H_2O$: C, 30.88; H, 6.69; N, 4.50. Found: C, 30.95; H, 6.77; N, 4.45. Anal. Calcd for $(Et_4N)_6[DyV_9O_{27}]\cdot H_2O$: C, 31.12; H, 6.64; N, 4.54. Found: C, 31.02; H, 6.68; N, 4.62. IR (Nujol, 500−1000 cm^{-1}): **5**, 946(s), 931(s), 900(s), 835(s), 781(s), 721(m), 665(s), 655(s); **6**, 970(sh), 927(s), 900(s), 838(s), 802(sh), 790(s), 721(m), 665(s), 655(s), 628(sh), 593(sh).

*Preparation of $(Et_4N)_5[(H_2O)Ho^{III}(V_4O_{12})_2]$ (**7**).* This compound was prepared similarly to **5** by using $(Et_4N)_4[V_4O_{12}]$ (240 mg, 1.05 mmol) and 0.095 mmol of anhydrous $HoCl_3$ (25.7 mg). Yield: ca. 233 mg (78.2% based on Ho). Anal. Calcd for $(Et_4N)_5[(H_2O)\text{-}HoV_8O_{24}]$: C, 29.55; H, 6.32; N, 4.31. Found: C, 29.31; H, 6.50; N, 4.40. IR (Nujol, 500−1000 cm^{-1}): 935(s), 917(s), 887(s), 819(s), 792(s), 721(sh), 690(s), 665(s).

*Preparation of $(Et_4N)_7[LnV_{10}O_{30}]$ [Ln = Er^{III} (**8**), Tm^{III} (**9**), Yb^{III} (**10**), Lu^{III} (**11**)].* These compounds were prepared similarly to **5** by using $(Et_4N)_4[V_4O_{12}]$ (240 mg, 1.05 mmol) and 0.09 mmol of anhydrous $LnCl_3$ ($ErCl_3$, 24.6 mg; $TmCl_3$, 24.8 mg; $YbCl_3$, 25.1 mg; $LuCl_3$, 25.3 mg) in acetonitrile (2 mL). Yield: ca. 120 mg (61% based on Ln). Anal. Calcd for $(Et_4N)_7[ErV_{10}O_{30}]\cdot 7H_2O$: C, 30.65; H, 7.07; N, 4.74. Found: C, 30.57; H, 6.97; N, 4.57. Anal. Calcd for $(Et_4N)_7[TmV_{10}O_{30}]\cdot 5H_2O$: C, 31.14; H, 7.00; N, 4.54. Found: C, 30.96; H, 7.15; N, 4.67. Anal. Calcd for $(Et_4N)_7[YbV_{10}O_{30}]\cdot 3H_2O$: C, 31.60; H, 6.91; N, 4.61. Found: C, 31.60; H, 7.08; N, 4.69. Anal. Calcd for $(Et_4N)_7[LuV_{10}O_{30}]\cdot 9H_2O\cdot 2CH_3CN$: C, 31.06; H, 7.12; N, 5.43. Found: C, 31.06; H, 7.03; N, 5.37. IR (Nujol, 500−1000 cm^{-1}): **8**, 933(s), 917(s), 885(s), 819(s), 792(s), 688(s), 665(s), 640(m); **9**, 935(sh), 919(s), 881(m), 869(sh), 821(s), 808(sh), 790(m), 779(m), 721(s), 674(s), 665(s), 626(sh); **10**, 935(s), 917(s), 883(m), 827(sh), 821(s), 790(m), 721(sh), 682(s), 665(s); **11**, 935(m), 917(m), 883(m), 827(s), 792(s), 721(sh), 682(s), 665(s).

Instrumentation. Elemental analyses were performed by the Kanazawa University Chemical Analysis Service. IR spectra were recorded as Nujol mulls between KBr plates on a Horiba FT-720 spectrophotometer. ^{51}V NMR spectra were recorded on a JEOL JNM-LA400 at 105.04 MHz. All NMR samples were measured in a CH_3CN solution. Chemical shifts were externally referenced to neat $VOCl_3$ (δ = 0 ppm). A 10-μs pulse width and a 10-μs preacquisition delay were used for all ^{51}V NMR measurements.

X-ray Crystallography. All crystals were extremely hygroscopic and were isolated in oil to avoid moisture and then mounted in a Hamilton cryoloop under a constant nitrogen flow. Several attempts to measure the crystal structures were carried out, and the best results are presented here. Intensity data for the crystals were collected at −150 °C on a Rigaku/MSC Mercury diffractometer with graphite-monochromated Mo Kα radiation (λ = 0.710 70 Å) using 0.5° ω scans at 0 and 90° in ϕ. Information on data collection and structure refinement, including the final cell constants, are summarized in Table 1, and additional information is available as CIF in the Supporting Information.

Data were collected and processed using the *CrystalClear* program (Rigaku). Face-indexed numerical absorption corrections were applied by the *CrystalClear* program. The data were corrected for Lorentz and polarization effects. The structure was solved by direct methods (*SHELXS-86*).[27] The non-hydrogen atoms were refined anisotropically. All compounds were refined without hydrogen atoms. Some $(Et_4N)^+$

dx.doi.org/10.1021/ic200638f | *Inorg. Chem.* 2012, 51, 784−793

Table 1. Crystal Data for 1, 2, and 5−11

	1·CH_3CN	**2**·CH_3CN	**5**·CH_3CN	**6**·$4CH_3CN$	**7**·$4CH_3CN$	**8**·$2CH_3CN$	**9**·$2CH_3CN$	**10**·$2CH_3CN$	**11**·$2CH_3CN$
formula	$C_{50}H_{123}N_7NdO_{27}V_9$	$C_{50}H_{123}N_7O_{27}SmV_9$	$C_{50}H_{123}N_7O_{27}TbV_9$	$C_{56}H_{132}N_{16}DyO_{27}V_9$	$C_{48}H_{114}HoN_9O_{25}V_8$	$C_{60}ErH_{146}N_9O_{30}V_{10}$	$C_{60}H_{146}N_9O_{30}TmV_{10}$	$C_{60}H_{146}N_9O_{30}V_{10}Yb$	$C_{60}H_{146}LuN_9O_{30}V_{10}$
fw	1857.26	1863.38	1871.94	1998.69	1789.94	2150.52	2152.19	2156.30	2158.23
cryst syst	orthorhombic	orthorhombic	orthorhombic	monoclinic	monoclinic	monoclinic	monoclinic	monoclinic	monoclinic
space group	$P2_12_12_1$ (No. 19)	$P2_12_12_1$ (No. 19)	$P2_12_12_1$ (No. 19)	$P2_1/c$ (No. 14)	$P2_1/n$ (No. 14)	$P2_1/n$ (No. 14)	$P2_1/n$ (No. 14)	$P2_1/n$ (No. 14)	$P2_1/n$ (No. 14)
a/Å	18.904(2)	18.925(3)	18.880(2)	23.693(2)	19.080(8)	15.015(1)	14.988(2)	15.052(2)	15.042(2)
b/Å	19.277(2)	19.256(3)	19.300(2)	44.032(4)	21.551(8)	14.737(1)	14.689(2)	14.790(1)	14.778(2)
c/Å	45.563(4)	45.494(6)	45.310(5)	25.265(3)	19.928(8)	21.531(2)	21.532(2)	21.408(2)	21.426(3)
α/deg	90.00	90.00	90.00	90.00	90.00	90.00	90.00	90.00	90.00
β/deg	90.00	90.00	90.00	95.365(2)	112.743(11)	100.450(3)	100.612(3)	100.028(3)	100.103(5)
γ/deg	90.00	90.00	90.00	90.00	90.00	90.00	90.00	90.00	90.00
V/Å^3	16604(3)	16579(4)	16510(3)	26243(4)	7557(5)	4685.2(7)	4659.5(9)	4693.1(8)	4688.9(10)
Z	8	8	8	12	4	2	2	2	2
no. of data collected	154 229	83 932	88 087	122 979	53 311	47 339	36 785	42 903	35 821
no. of data used	19 569	16 119	15 835	37 776	14 341	10 141	9716	10 051	9559
no. of variables	1583	1482	1576	2708	948	584	584	584	584
R_1 $[I > 2\sigma(I)]$	0.0742	0.0687	0.0746	0.118	0.0714	0.0444	0.0416	0.0596	0.0586
R_{all} $[I > 2\sigma(I)]$	0.1058	0.0712	0.0814	0.1428	0.0909	0.0458	0.0423	0.0610	0.0610
wR_2	0.2026	0.1910	0.2041	0.2922	0.2033	0.1158	0.1045	0.1481	0.1448
GOF	0.996	1.074	1.073	1.053	1.056	1.067	1.061	1.073	1.134

dx.doi.org/10.1021/ic200638f | Inorg. Chem. 2012, 51, 784−793

cations and acetonitrile solvent molecules were observed with the presence of disorders and treated with partial occupancy. The *SHELXL-93* program was used for full-matrix least-squares refinement.[28] All calculations were performed using the *teXsan* crystallographic software package of Molecular Structure Corp.[29] After the refinements, the *PLATON* program was used to confirm the accuracy of the refinements, space group choice, and lack of higher symmetry.[30]

EXAFS Measurements. The lanthanide L_{III}-edge EXAFS measurements for solid samples and acetonitrile solution samples were performed at 295 K using the BL-3 and BL-4 at the SR Center of Ritsumeikan University.[31] All samples were prepared in an anaerobic environment using a polyethylene glovebag filled with dry nitrogen because of the extreme hygroscopic nature of the sample. Solid samples were diluted with boron nitride and pressed into pellets of 20 mm diameter. The pellets were sealed in a polyethylene bag in order to avoid moisture. Sample solutions with lanthanide concentrations of 0.1 mol dm^{-3} were prepared by dissolving the powder of each complex with n-Bu_4NBF_4 in acetonitrile at 323 K. The solution samples were absorbed in dried glass fiber filters, which were sealed in a polyethylene bag to avoid moisture and prevent evaporation of acetonitrile. The white synchrotron radiations were monochromatized by a Si(220) double-crystal monochromator. Data collections of the L_{III}-edge absorption edges were performed in transmission mode. The incident (I_0) and transmitted X-ray intensities (I) were simultaneously measured by ionization chambers with lengths of 4.5 and 31 cm, respectively. The ionization chamber for the transmitted intensity measurements (I_0) was filled with N_2 (85%) and Ar (15%) gases for measurements of the L_{III} edges (Nd, Sm, Eu, Gd, Tb, Dy, and Ho) and with N_2 (50%) and Ar (50%) gases for measurements of the L_{III} edges (Er, Tm, Yb, and Lu). The ionization chamber for the I measurements was filled with N_2 (50%) and Ar (50%) gases throughout the experiments.

The threshold energy of a L_{III}-shell electron, E_0, was selected as the position of half-height of the edge jump in each sample. The background absorption was estimated by the least-squares fittings of the Victoreen formulas to the observed data in the preedge region and was subtracted from the total absorption in the postedge region by extrapolation. The smooth L_{III}-shell absorption was evaluated by fitting of the cubic spline function. The extraction and normalization of the EXAFS oscillation $\chi(k)$ were performed with the program *REX2000*[32] as a function of the wavenumber (k) of the ejected photoelectron. The radial structural functions were obtained by the Fourier transformation of k^3-weighted EXAFS oscillations. The structural parameters were determined by the least-squares fittings of the theoretical EXAFS function in r space using the program *Artemis*.[33] The model EXAFS function is simply written by eq 1,[34]

$$\chi_{calc}(k) = \sum_j {S_0}^2 n_j \frac{F_j(k)}{k{r_j}^2} \sin[2r_j k + \delta_j(k)] \exp\left(-2k^2/{\sigma_j}^2 - \frac{2r_j}{\lambda_j(k)} \right) \quad (1)$$

where $F_j(k)$ is the effective single-scattering amplitude from each of the n_j scatterers at a distance r_j from the X-ray-absorbing atom for the jth path, $\delta_j(k)$ is the total phase shift, $\lambda_j(k)$ is the mean free path of the photoelectron, and ${S_0}^2$ is the overall amplitude reduction factor. The EXAFS parameters of $F_j(k)$, $\delta_j(k)$, and $\lambda_j(k)$ were taken from FEFF 6[35] calculations for the models of the atomic coordinates obtained by X-ray crystallography. Because of the lack of good crystallographic data for europium and gadolinium complexes, their atomic coordinates were substituted by the data from isomorphous crystals of samarium and terbium complexes, respectively. The Ln−O and Ln···V single scattering and the multiple scattering for a path of Ln−O···V were taken into account for each complex. The multiple scattering for a path of Ln−O···O−Ln was not included in the fitting procedure because its contribution was much smaller.

RESULTS AND DISCUSSION

Lanthanide-incorporated polyoxovanadates have been synthesized by the reaction of $[V_4O_{12}]^{4-}$ and a lanthanide chloride in acetonitrile. The synthetic procedure is straightforward for the series of complexes. The solubility of lanthanide chlorides of neodymium, samarium, europium, and gadolinium in acetonitrile is low, but stirring the mixture allows for dissolution of the chlorides and produces a faint-purple solution. After the unreacted precipitate is removed by filtration, the solution is concentrated for crystallization, giving colorless crystals except in the case of the neodymium complex **1**, which is a faint-blue color. For the reaction with the later series of lanthanide chlorides (Ln = Tb, Dy, Ho, Er, Tm, Yb, and Lu), which have a higher solubility in acetonitrile, nearly colorless solutions are produced except in the case of the erbium complex, which is a pale-red color, and crystals are formed by evaporation of the solvent or storage at cold temperature. The addition of a 10-fold excess of metavanadate against lanthanide ions is required to prevent the formation of large amounts of insoluble precipitates. The exclusion of water or alcohol from the solvent is important for the synthesis; otherwise, yellow orange precipitates, which are unidentified decomposition products, are formed. However, a trace amount of water in acetonitirile does not affect the synthesis. The isolated crystals are extremely hygroscopic.

The IR spectra of the lanthanide complexes exhibit characteristic peaks between 1000 and 400 cm^{-1} due to V−O stretches, and each series of complexes shows a similar pattern in the spectra (see the Supporting Information). The higher-energy regions are assigned to terminal V−O stretches, whereas the lower-energy regions correspond to bridging V−O stretches. The spectra of **1**−**6** show two sets of strong bands in the 950−850 and 850−750 cm^{-1} regions. The V−O peaks are broader in the spectra of **7**−**11** and the two regions are overlapped, as a result of the greater variety of bonding modes compared to **1**−**6** with more rigid structures.

Three different types of structures are observed in the series of complexes **1**−**11**. The structure of $[LnV_9O_{27}]^{6-}$ [Ln = Nd (**1**), Sm (**2**), Eu (**3**), Gd (**4**), Tb (**5**), Dy (**6**)] is shown in Figure 1. It is composed of nine tetrahedral VO_4 units linked to each other by vertex sharing to form a macrocyclic $[V_9O_{27}]^{9-}$ ring. At the center, a lanthanide ion exists with a square-antiprism coordination environment. The coordination of eight VO_4 units through oxido atoms is observed, and each of the vanadium atoms has one terminal oxygen atom. The coordinated VO_4 tetrahedral units are alternately up and down relative to the plane of the V_9 ring, which is perpendicular to the 4-fold axis of the square-antiprism coordination, as seen in Figure 1. Among the nine VO_4 tetrahedra, one unit is free from coordination to the lanthanide ion, leaving two terminal V−O bonds at the vanadium atom. The average Ln−O bond distance is in the normal range for square-antiprism lanthanide ions. Interestingly, despite the trend of decreasing ionic radii by the lanthanide contraction, $[LnV_9O_{27}]^{6-}$-type complexes **1**−**6** adopt the same structure composed of a $[V_9O_{27}]^{9-}$ ligand. The crystal packings show two identical molecules in an asymmetric unit in complexes **1**, **2**, and **5** (Figures S5−S10 in the Supporting Information). The poor quality of crystals **3** and **4** does not allow for good refinements because of the severe disorder of countercations and solvents; however, crystals **3**, **4**,

dx.doi.org/10.1021/ic200638f | Inorg. Chem. 2012, 51, 784−793

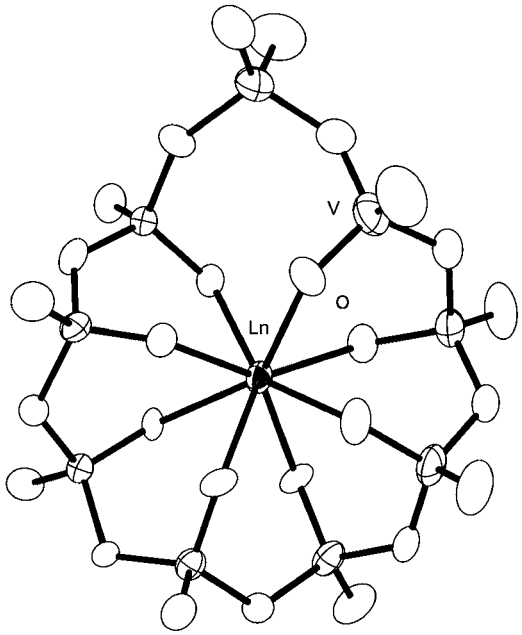

Figure 1. ORTEP representation of anion **1** with thermal ellipsoids drawn at the 50% probability level. The structure of **1** represents the structures of **2**, **3**, and **6**. Equatorial-octant, equatorial, and hollow ellipsoids represent lanthanide, vanadium, and oxygen atoms, respectively.

and **6** are isomorphous, and thus identical structures of complexes **3** and **4** with **6** are expected (see also the discussion in the EXAFS observation).[36] Complexes **1**, **2**, and **5** are also isomorphous. Complexes **3**, **4**, and **6** exhibit three identical units in an asymmetric unit (Figures S11 and S12 in the Supporting Information).

Complex **7**, $[(H_2O)Ho^{III}(V_4O_{12})_2]^{5-}$, exhibits a structure different from the rest of the compounds (Figure 2). Two sets of tripod coordinations of the tetravanadate, $[V_4O_{12}]^{4-}$, bind the Ho^{III} ion to form a capped trigonal-prism coordination environment with additional coordination of a water ligand at the capped position. One VO_4 unit on each of the tetravanadates is not coordinated to the Ho^{III} ion and has two terminal oxygen atoms that interact with the capping water ligands through hydrogen bonds [O···O distances, 2.688(9) and 2.698(9) Å].

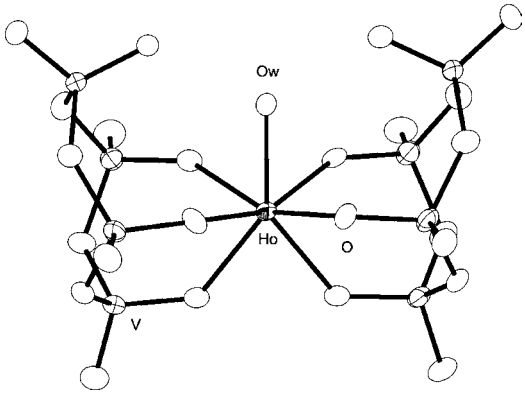

Figure 2. ORTEP representation of anion **7** with thermal ellipsoids drawn at the 50% probability level. Equatorial-octant, equatorial, and hollow ellipsoids represent holmium, vanadium, and oxygen atoms, respectively.

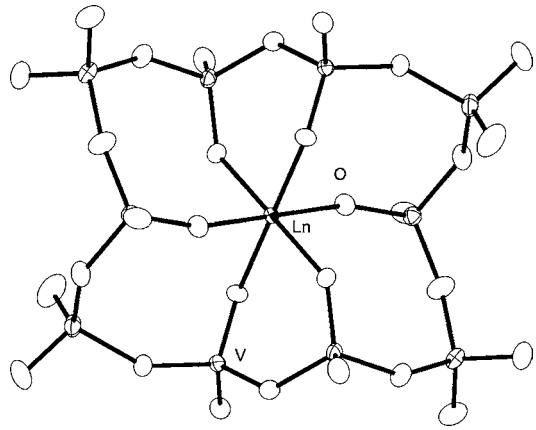

Figure 3. ORTEP representation of anion **11** with thermal ellipsoids drawn at the 50% probability level. The structure of **11** represents the isomorphous structures of **8**–**10**. Equatorial-octant, equatorial, and hollow ellipsoids represent lanthanide, vanadium, and oxygen atoms, respectively.

The structure of $[LnV_{10}O_{30}]^{7-}$ [Ln = Er (**8**), Tm (**9**), Yb (**10**), Lu (**11**)] is shown in Figure 3. Complexes **8**–**11** are isomorphous, and an asymmetric unit contains one anion, seven tetraethylammonium cations, and one acetonitrile molecule. The 10 VO_4 units form a macrocyclic ligand similar to a crown ether, and six VO_4 units are coordinated to the lanthanide ion at the center of an octahedral coordination site. The octahedral site is close to an ideal regular octahedron without distortion [Ln–O distances: Er, 2.2187(1)–2.2548(1) Å; Tm, 2.2045(2)–2.2457(2) Å; Yb, 2.1917(1)–2.2335(1) Å; Lu, 2.190(4)–2.216(3) Å. O–Ln–O angles: Er, 88.31(9)–91.69(9)°; Tm, 88.01(8)–91.99(8)°; Yb, 88.73(13)–91.27(13)°; Lu, 88.6(1)–91.4(1)°]. The four VO_4 units at the corner of the squarelike arrangement of the V_{10} ring in Figure 3 are not coordinated to the lanthanide ion and have two terminal oxygen atoms on the free VO_4 unit.

Two types of disk-shaped macrocyclic heteropolyoxovanadates are observed: one for the early lanthanide complexes, $[LnV_9O_{27}]^{6-}$ [Ln = Nd (**1**), Sm (**2**), Eu (**3**), Gd (**4**), Tb (**5**), Dy (**6**)], and the other for the later lanthanide complexes, $[LnV_{10}O_{30}]^{7-}$ [Ln = Er (**8**), Tm (**9**), Yb (**10**), Lu (**11**)]. The early lanthanide complexes **1**–**6** adopt eight-coordinated square-antiprism structures, and the later lanthanides **8**–**11** adopt six-coordinated octahedral structures. The trend of decreasing the coordination number is consistent with the change of the ionic radii based on the lanthanide contraction. At the boundary, the Ho^{III} ion exhibits a completely different structure, a seven-coordinated capped trigonal-prism coordination. This is probably due to the unsuitable ionic radius of the Ho^{III} ion, which is too small for an eight-coordination site and too large for a six-coordination site. Interestingly, each series of complexes **1**–**6** or complexes **8**–**11** can adopt the same structure despite variation of the ionic radii among the different lanthanide ions. The flexibility of these macrocyclic polyoxovanadates due to the linkages of the VO_4 units can be explained by the tortion angle of O–V···V–O defined in Figure 4, where the binding coordination of vertex-shared VO_4 units to a lanthanide ion through the oxido ligands is depicted. Smaller torsion angles for smaller lanthanides, and larger torsion angles for larger lanthanides, are observed, as shown in Table 2. By a smooth adjustment of the conformation of the ring, the cyclic

dx.doi.org/10.1021/ic200638f | Inorg. Chem. 2012, 51, 784–793

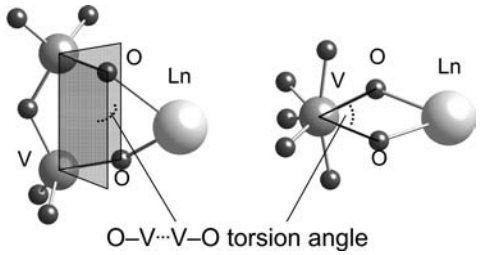

Figure 4. Schematic drawing of the binding of vertex-shared VO_4 units as bidentate ligands to a lanthanide ion. The definition of the torsion angle of O–V···V–O is designated by a dotted line. Left: top view. Right: side view from the V···V axis. By adjustment of the torsion angle shown here, the $(VO_3)_n^{n-}$ ligands can bind a range of different sizes of lanthanide ions without a large change in the VO_4 tetrahedral units, with accompanying changes of the Ln–O lengths to fit the different ionic radii.

polyoxovanadates can accommodate ions of different sizes. The three different types of structures adopt a different range of tortion angles. Complex **1** has the largest ionic radius in the series and an average torsion angle of 49.2°. The angle continuously decreases across the nine-membered vanadium structures in the series of the early lanthanides, and in the dysprosium complex **6**, the angle becomes 46.8°. In the later series of the 10-membered vanadium complexes, the erbium complex **8** has a smaller torsion angle of 23.88°, which also continuously decreases down to 23.1° for the lutetium complex **11**. These variations in torsion angles enable slight modifications of the ring conformation, which enable the different ionic radii to fit without distortion of the VO_4 units. The geometrical parameters of the VO_4 units do not deviate greatly from the standard values in that the V–$O_{terminal}$ and V–μ-O bond lengths are similar across the series of complexes (average V–μ-O lengths: Nd, 1.80(1); Sm, 1.81(1); Tb, 1.81(2); Dy, 1.80(3); Ho, 1.803(6); Er, 1.7989(1); Tm, 1.7978(2); Yb, 1.7985(1); Lu, 1.798(4) Å), even though accompanying changes of Ln–O and Ln···V distances and Ln–O–V angles are observed to accept the different sizes of the lanthanide ions (Table 2). Complex **7** has the smallest torsion angle of 11.6°, reflecting the flat coordination needed to sandwich the Ho^{III} ion by the flat $[V_4O_{12}]^{4-}$ units. Despite the fairly constant geometry of the VO_4 units, the different cation sizes can be accommodated within the macrocyclic ligand by simply adjusting the torsion angles. These series of novel all-inorganic lanthanide complexes resemble crown ethers and exhibit fairly flexible inorganic cyclic ligand systems.

The structures of europium and gadolinium complexes (**3** and **4**) could not be refined by X-ray structure analysis because of the poor quality of the crystals; thus, their structures were evaluated through EXAFS studies. The EXAFS analyses were also performed to gain insight as to whether the solid-state structures of these macrocyclic polyoxovanadate complexes are maintained in solution. Figure 5 shows a comparison of the EXAFS oscillations

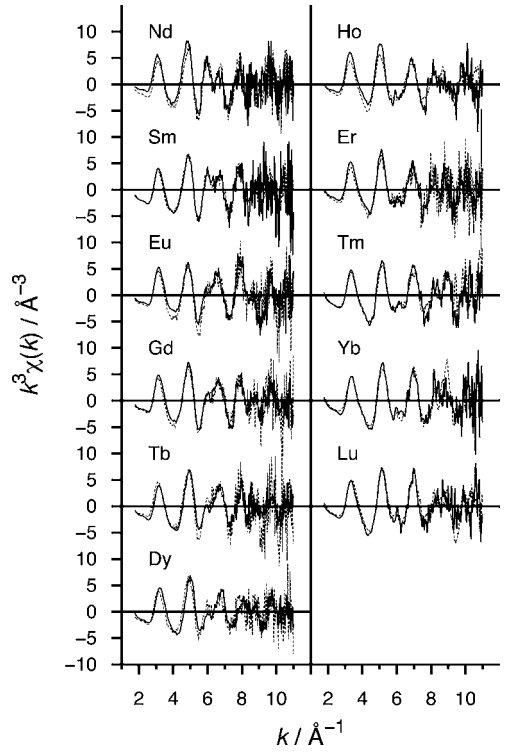

Figure 5. Ln L_{III}-edge $k^3\chi(k)$ EXAFS oscillations for complexes **1**–**11**. Solid line: solid-state samples. Dotted line: samples in acetonitrile.

between the solid and solution samples of each of the complexes. Identical oscillation patterns are observed in the solid and solution states throughout the series of complexes, which clearly indicate the retention of the structures in an acetonitrile solution. Figure 6 shows the FT magnitudes of each of the solid samples with curve fittings (for solution samples, see the Supporting Information). In both the solid-state and solution samples, two peaks centered at ca. 1.9 and 3.3 Å are clearly observed, which are assigned to the Ln–O and Ln···V vectors, respectively. A comparison of the intensity ratios between the two regions reveals a greater intensity ratio for the second sphere of complexes **1**–**6**, which have more rigid structures; that is, eight vanadium units are fixed by coordination to the lanthanide ion. For complexes **8**–**11**, the peak intensity of the second coordination sphere is weaker because the presence of free VO_4 units liberates the Ln···V distances. In these structures, four VO_4 units of the 10-membered

Table 2. Comparison of the Structure Parameters for the Series of Lanthanide Complexes

complex	mean Ln–O distances/Å	mean Ln–V distances/Å	mean V–O_{Ln} distances/Å	mean V–$O_{terminal}$ distances/Å	mean Ln–O–V angles/deg	mean O–V···V–O torsion angles/deg
1	2.445(8)	3.756(2)	1.662(9)	1.621(10)	131.5(5)	49.2(4)
2	2.420(8)	3.740(2)	1.660(9)	1.63(1)	132.1(5)	48.4(4)
5	2.392(18)	3.719(4)	1.66(2)	1.63(2)	133.0(1)	47.8(9)
6	2.378(20)	3.709(6)	1.66(2)	1.63(3)	133.0(1)	46.8(10)
7	2.313(5)	3.7472(4)	1.674(7)	1.614(6)	140.5(3)	11.6(3)
8	2.2317(1)	3.6758(3)	1.6770(1)	1.6277(1)	141.32(-)	23.88(-)
9	2.2195(2)	3.6669(3)	1.6750(1)	1.6280(1)	141.73(-)	23.63(-)
10	2.2083(1)	3.6572(3)	1.6795(1)	1.6247(1)	141.53(-)	23.34(-)
11	2.199(3)	3.6531(6)	1.678(3)	1.628(4)	142.0(2)	23.1(2)

dx.doi.org/10.1021/ic200638f | *Inorg. Chem.* 2012, 51, 784–793

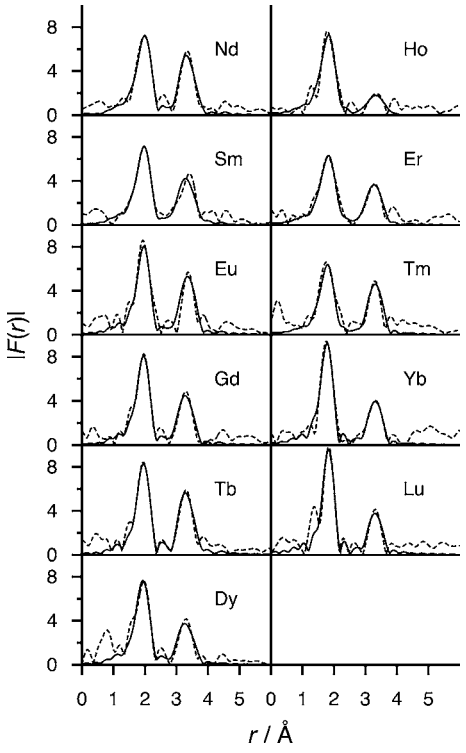

Figure 6. Radial structural functions for complexes **1**−**11** in the solid state. Solid line: simulated data. Dotted line: experimental data.

vanadium ring are not coordinated, implying larger thermal motions on the vanadium atoms, causing weaker intensities at the second coordination sphere. In the curve fittings, the coordination numbers of the complexes were fixed to the results derived from the X-ray crystal data. This enabled us to focus on the estimation of the bond-length parameters. This can decrease the error from the influence of multielectron transitions, which has been known to cause approximately 10% error for coordination numbers in the EXAFS data analysis of rare-earth systems.[37] From the result of curve fittings with estimation of the multiscattering effects, the estimated distances of Ln−O and Ln···V are listed in Tables 3 and 4. Remarkable agreement of the bond lengths between the data from the crystal structure and EXAFS observations is observed. In addition, the data for the solid-state and solution samples agree quite well in EXAFS oscillations, confirming the homogeneity of the solid sample and the structure retention in solution. From a comparison of the EXAFS data, the assumption made for the structures of complexes **3** and **4** that they have the same structure as the neodymium complex **1** is justified. Figures 7 and 8 show plots of the ionic radii of the lanthanide ions[38] corresponding to the observed coordination number versus the estimated bond lengths of Ln−O and Ln···V, respectively, in the complexes. Linear relationships are observed in both plots despite the resulting structure adopted, suggesting the high flexibility of these cyclic ligands in the choice of three types of structures. The three types of structures are arranged in three separate groups in

Table 3. Estimated Ln−O Bond Lengths by EXAFS and Corresponding X-ray Data for Lanthanide Complexes

	EXAFS(solid)			EXAFS(solution)			crystal data[d]
Ln−O	CN[a]	r^b/Å	$\sigma^{2\,c}$/Å^2	CN[a]	r^b/Å	$\sigma^{2\,c}$/Å^2	r/Å
Nd−O	8	2.46(2)	0.011(2)	8	2.47(1)	0.013(3)	2.445(8)
Sm−O	8	2.44(1)	0.012(2)	8	2.47(1)	0.011(2)	2.420(8)
Eu−O	8	2.41(2)	0.008(2)	8	2.39(2)	0.007(2)	
Gd−O	8	2.40(1)	0.008(2)	8	2.39(1)	0.011(2)	
Tb−O	8	2.39(1)	0.007(1)	8	2.37(1)	0.013(2)	2.392(18)
Dy−O	8	2.38(1)	0.010(2)	8	2.33(1)	0.010(2)	2.378(20)
Ho−O	7	2.28(2)	0.011(2)	7	2.29(1)	0.009(2)	2.313(5)
Er−O	6	2.27(2)	0.013(2)	6	2.27(2)	0.011(2)	2.2317(1)
Tm−O	6	2.23(2)	0.011(3)	6	2.22(1)	0.007(2)	2.2195(2)
Yb−O	6	2.20(1)	0.006(2)	6	2.24(1)	0.009(2)	2.2083(1)
Lu−O	6	2.22(1)	0.004(2)	6	2.21(1)	0.010(2)	2.199(3)

[a]Coordination number (fixed). [b]Distances between Ln and O. [c]Debye−Waller factor. [d]Mean distances.

Table 4. Estimated Ln···V Bond Lengths and Corresponding X-ray Data for Lanthanide Complexes

	EXAFS(solid)			EXAFS(solution)			crystal data[d]
Ln···V	CN[a]	r^b/Å	$\sigma^{2\,c}$/Å^2	CN[a]	r^b/Å	$\sigma^{2\,c}$/Å^2	r/Å
Nd···V	8	3.76(2)	0.011(2)	8	3.76(3)	0.014(2)	3.756(2)
Sm···V	8	3.741(8)	0.013(1)	8	3.77(3)	0.013(2)	3.740(2)
Eu···V	8	3.75(3)	0.009(2)	8	3.74(4)	0.009(2)	
Gd···V	8	3.72(2)	0.010(2)	8	3.74(3)	0.013(2)	
Tb···V	8	3.72(2)	0.007(1)	8	3.74(4)	0.014(2)	3.719(4)
Dy···V	8	3.72(3)	0.012(2)	8	3.73(5)	0.013(2)	3.709(6)
Ho···V	6	3.71(6)	0.016(5)	6	3.65(3)	0.012(2)	3.7472(4)
Er···V	6	3.66(4)	0.012(2)	6	3.65(4)	0.013(3)	3.6758(3)
Tm···V	6	3.66(6)	0.009(2)	6	3.62(4)	0.009(2)	3.6669(3)
Yb···V	6	3.65(3)	0.009(2)	6	3.64(3)	0.012(2)	3.6572(3)
Lu···V	6	3.65(5)	0.007(2)	6	3.67(4)	0.015(3)	3.6531(8)

[a]Coordination number (fixed). [b]Distances between Ln and V. [c]Debye−Waller factor. [d]Mean distances.

dx.doi.org/10.1021/ic200638f | Inorg. Chem. 2012, 51, 784−793

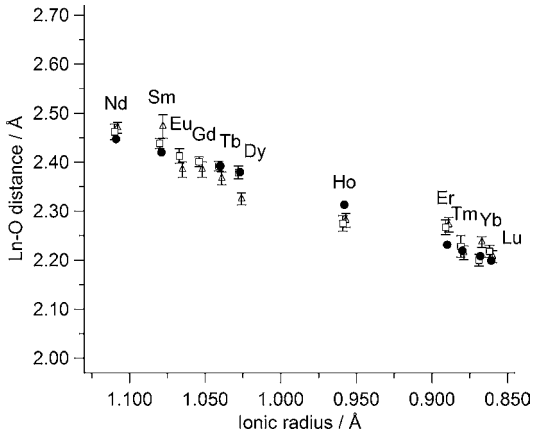

Figure 7. Plot of mean Ln−O distances for complexes **1**−**11**. Black circles: X-ray crystal data. Squares: EXAFS data in the solid state. Triangles: EXAFS data in an acetonitrile solution.

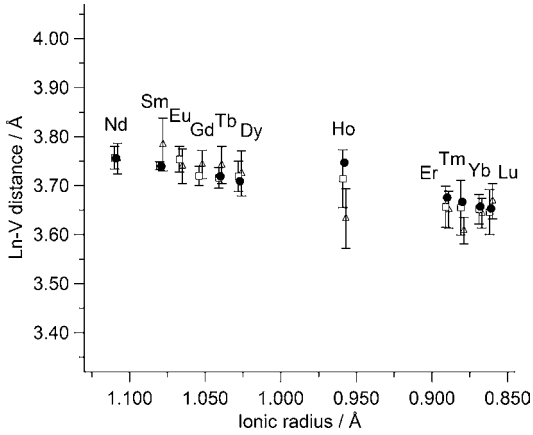

Figure 8. Plot of mean Ln···V distances for complexes **1**−**11**. Black circles: X-ray crystal data. Squares: EXAFS data in the solid state. Triangles: EXAFS data in an acetonitrile solution.

the plot. The early lanthanide complexes with ionic radii in the range 1.02−1.15 Å adopt the eight-coordination structure of the nine-membered vanadium ring, and the later lanthanide complexes with ionic radii in the range 0.85—0.9 Å adopt the six-coordination structure of the 10-membered vanadium ring. Complex **7** is in the middle of the two groups. The cyclic polyoxovanadate structures can accept a certain range of ionic radii by slight modification of their conformations, and the gap on both sides of the Ho^{III} ion shows the borderline to adopt a different structure. From the plots, good agreements between solid-state and solution bond lengths are observed, which also match well with the average bond lengths from the X-ray structures. Part of the reason that these excellent agreements can be observed is because of the rigid cyclic structure of these complexes, which have similar Ln−O bond lengths and Ln···V interatomic distances arising from the disklike cluster geometry. The larger standard deviation of Ho···V lengths observed in the holmium complex **7** is due to coordination of the additional water ligand, which likely dissociates in acetonitrile, causing the shorter estimation of the Ln···V bond length in an acetonitrile solution.

Preliminary experiments were performed to determine the effect of the addition of water to the acetonitrile solution. The intensity of the second coordination sphere peak in the FT magnitudes of the dysprosium complex **6** is decreased when the sample is exposed to air or water, but the peak at the first coordination sphere is still observed (see Figure S4 in the Supporting Information). This indicates that part of the macrocyclic ligand is dissociated from the lanthanide ion, yet the coordination of Dy−O is still intact, implying the accompanying dissociation of the VO_4 units and coordination of the added water molecule, as seen in the structure of the $[Co_2(H_2O)_2(V_{10}O_{30})]^{6-}$ ion.[24] Partial dissociation of the VO_4 units and additional coordination of the water ligand to the lanthanide ion may be possible in these cyclic polyoxovanadate systems.

Figure 9 shows variable-temperature ^{51}V NMR spectra of the neodymium compex **1** in an acetonitrile solution. Four distinct

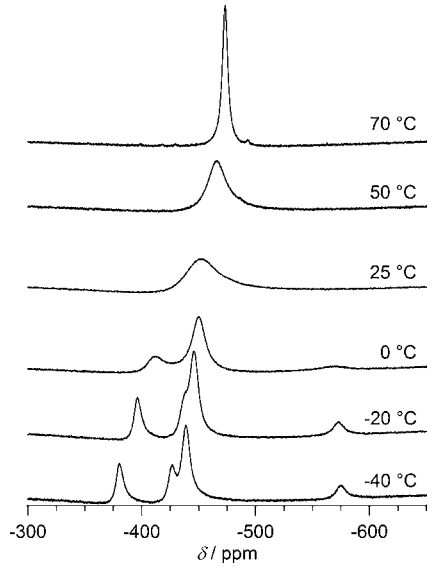

Figure 9. Variable-temperature ^{51}V NMR spectra of complex **1** in acetonitrile.

peaks were observed at −40 °C with an intensity ratio of 2:2:4:1 at −380, −426, −438, and −572 ppm. The chemical environment of the nine-membered vanadium ring has one noncoordinating VO_4 unit and four pairs of equivalent VO_4 units that are coordinated to the lanthanide ion. From the intensity ratio, the most upfield field peak at −572 ppm can be assigned to the noncoordinated unit, and the rest of the four environments are observed with a 2:2:4 ratio. The number of chemical environments based on the structure and the intensity ratio matched the X-ray structure, but the detailed assignments of the individual signals are difficult at the current stage. At 70 °C, all of the signals converge to a single peak at −473 ppm. The convergence of the signal suggests dynamic chemical equilibrium of the cyclic structure, and all of the vanadium sites become equivalent at the higher temperature. These changes were reversible within this temperature range without decomposition. The suggested mechanism is shown in Figure 10. The VO_4 unit immediately adjacent to the noncoordinated VO_4 unit dissociates, and then the noncoordinated VO_4 unit recoordinates to the lanthanide ion, resulting in a shift of the position of the noncoordinated VO_4 unit. The alternate shifts of a noncoordinated unit average out the chemically inequivalent sites on the nine-membered vanadium ring. The EXAFS studies confirm that the structure in acetonitrile is the same as the crystal structure at the longer time scale, and the stepwise shift of the coordination sites explains the temperature dependence of the NMR spectra.

dx.doi.org/10.1021/ic200638f | Inorg. Chem. 2012, 51, 784−793

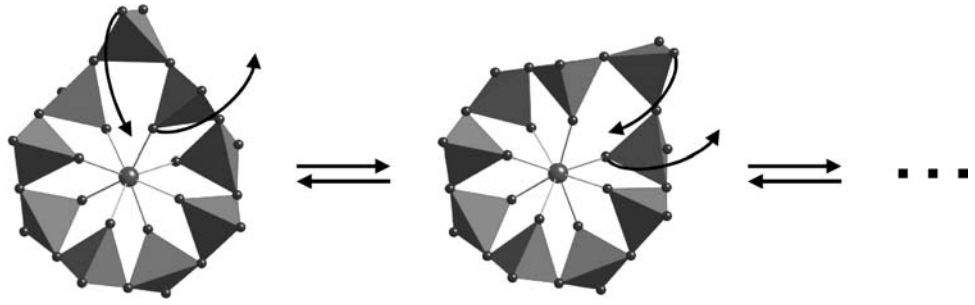

Figure 10. Proposed dynamic behavior of complex **1** in acetonitrile. In the V_9 ring, the noncoordinated VO_4 unit may alternately flip to dissociate from the lanthanide ion and the next coordinated VO_4 unit associates, resulting a shift of the noncoordinated unit around the ring.

CONCLUSIONS

We have synthesized three types of lanthanide-incorporated heteropolyoxovanadates, and the trend of adopted structures correlates with the decreasing trend of ionic radii, i.e., a larger coordination number structure for larger ions and a smaller coordination number structure for smaller ions. The flexibility of the cyclic polyoxovanadate ligands composed by the vertex sharing of VO_4 units can accommodate a range of lanthanide ions with different ionic radii by adjusting the torsion angles between the VO_4 tetrahedral units. The larger ions for the early lanthanide complexes, $[LnV_9O_{27}]^{6-}$ [Ln = Nd (**1**), Sm (**2**), Eu (**3**), Gd (**4**), Tb (**5**), Dy (**6**)] exhibit a structure with a nine-membered vanadium ring with a square-antiprism coordination sphere. The smaller ions for the later lanthanide complexes, $[LnV_{10}O_{30}]^{7-}$ [Ln = Er (**8**), Tm (**9**), Yb (**10**), Lu (**11**)], adopt an octahedral coordination mode with a 10-membered vanadium ring in which four of the VO_4 units are not coordinated to the lanthanide ion. The Ho^{III} complex, $[(H_2O)Ho^{III}(V_4O_{12})_2]^{5-}$ (**7**), has a boundary ionic radius for those rings, adopting a sandwiched structure by two tridentate tetravanadate units, which has a capped trigonal-pyramidal coordination with coordination of water at the capped position. EXAFS studies show clear patterns in the bond lengths of Ln−O and Ln···V, which can differentiate among the three types of structures. With estimation of the multiple scatterings, the agreement between the X-ray and EXAFS data both in the solid state and in acetonitrile is excellent by means of the bond lengths of the first and second coordination spheres. These lanthanide complexes of polyoxovanadates show retention of the structure in an acetonitrile solution, which is supported by the identical spectra of the EXAFS oscillation. ^{51}V NMR studies show the shift of a noncoordinated VO_4 site around the cyclic structure by alternating coordination of the VO_4 units at 70 °C, and this dynamic equilibrium also indicates the flexibility of the macrocyclic ligands. We now foresee possibilities of the formation of all-inorganic cyclic polyoxovanadates throughout the transition elements because the first transition metals and now the lanthanide series of complexes are established. Future studies on earlier lanthanide ions are in progress.

ASSOCIATED CONTENT

Supporting Information

Crystallographic data in CIF format, table of estimated Dy−O and Dy···V with exposure to air or water, IR data for **1**−**11**, EXAFS radial functions of **1**−**11** in acetonitrile, EXAFS functions of **6** by the effect of water addition, and ORTEP and packing diagrams of **1**, **2**, and **5**−**11**. This material is available free of charge via the Internet at http://pubs.acs.org.

AUTHOR INFORMATION

Corresponding Author

*E-mail: hayashi@se.kanazawa-u.ac.jp. Fax: (+81)76-264-5742.

ACKNOWLEDGMENTS

This work was supported by a Grant in Aid for Scientific Research and "Nanotechnology Network Project" of the Ministry of Education, Culture, Sports, Science and Technology (MEXT), Japan. We thank Professor Nomura Masaharu (High Energy Accelerator Research Organization, KEK) for helpful discussions.

REFERENCES

(1) (a) *Polyoxometalates: from Platonic Solids to Anti Retroviral Activity*; Pope, M. T., Müller, A., Eds.; Kluwer: Dordrecht, The Netherlands, 1994. (b) Hill, C. L., Ed. *Chem. Rev.* **1998**, *98*, 1−389 (special thematic issue on polyoxometalates). (c) *Polyoxometalate Chemistry: From Topology via Self-Assembly to Applications*; Pope, M. T., Müller, A., Eds.; Kluwer: Dordrecht, The Netherlands, 2001. (d) *Polyoxometalate Chemistry for Nano-Composite Design*; Yamase, T., Pope, M. T., Eds.; Kluwer: Dordrecht, The Netherlands, 2002. (e) Long, D. L.; Burkholder, E.; Cronin, L. *Chem. Soc. Rev.* **2007**, *36*, 105−121. (f) Kortz, U., Ed. *Eur. J. Inorg. Chem.* **2009**, *34*, 5053−5280 (special thematic issue on polyoxometalates).

(2) Kozhevnikov, I. V. *Catalysts for Fine Chemical Synthesis, Catalysis by Polyoxometalates*; Wiley: Chichester, U.K., 2002.

(3) (a) Preyssler, C. *Bull. Soc. Chim. Fr.* **1970**, 30. (b) Alizadeh, M. H.; Harmalker, S. P.; Jeannin, Y.; Martin-Frère, J.; Pope, M. T. *J. Am. Chem. Soc.* **1985**, *107*, 2662−2669.

(4) (a) Antonio, M. R.; Malinsky, J.; Soderholm, L. *Mater. Res. Soc. Symp. Proc.* **1995**, *368*, 223−8. (b) Antonio, M. R.; Soderholm, L. *J. Cluster Sci.* **1996**, *7*, 585−591. (c) Chiang, M.-H.; Williams, C. W.; Soderholm, L.; Antonio, M. R. *Eur. J. Inorg. Chem.* **2003**, 2663−2669. (d) Fernandez Jorge, A.; Lopez, X.; Bo, C.; de Graaf, C.; Baerends Evert, J.; Poblet Josep, M. *J. Am. Chem. Soc.* **2007**, *129*, 12244−53. (e) Fernandez, J. A.; Lopez, X.; Bo, C.; De Graaf, C.; Baerends, E. J.; Poblet, J. M. *J. Am. Chem. Soc.* **2007**, *129*, 12244−12253.

(5) (a) Lis, S.; But, S.; Klonkowski, A. M.; Grobelna, B. *Int. J. Photoenergy* **2003**, *5*, 233−238. (b) Lu, Y.; Li, Y.; Wang, E.; Xu, X.; Ma, Y. *Inorg. Chim. Acta* **2007**, *360*, 2063−2070.

(6) (a) Yamase, T.; Naruke, H. *J. Chem. Soc., Dalton Trans.* **1991**, 285−292. (b) Yamase, T. *Chem. Rev.* **1998**, *98*, 307−325. (c) Yamase, T.; Naruke, H. *J. Phys. Chem. B* **1999**, *103*, 8850−8857. (d) Granadeiro, C. M.; Ferreira, R. A. S.; Soares-Santos, P. C. R.; Carlos, L. D.; Nogueira, H. I. S. *Eur. J. Inorg. Chem.* **2009**, *34*, 5088−5095.

(7) Pope, M. T. *Heteropoly and Isopoly Oxometalates*; Springer: Berlin, 1983.

(8) (a) Peacock, R. D.; Weakley, T. J. R. *J. Chem. Soc. A* **1971**, 1836−1839. (b) Iball, J.; Low, J. N.; Weakley, T. J. R. *J. Chem. Soc., Dalton Trans.* **1974**, 2021−2024.

(9) Wassermann, K.; Dickman, M. H.; Pope, M. T. *Angew. Chem., Int. Ed. Engl.* **1997**, *36*, 1445−1448.
(10) (a) Kato, R.; Kobayashi, A.; Sasaki, Y. *J. Am. Chem. Soc.* **1980**, *102*, 6571−6572. (b) Kato, R.; Kobayashi, A.; Sasaki, Y. *Inorg. Chem.* **1982**, *21*, 240−246.
(11) Ichida, H.; Nagai, K.; Sasaki, Y.; Pope, M. T. *J. Am. Chem. Soc.* **1989**, *111*, 586−591.
(12) Liu, S.; Li, D.; Xie, L.; Cheng, H.; Zhao, X.; Su, Z. *Inorg. Chem.* **2006**, *45*, 8036−8040.
(13) (a) Konaka, S.; Ozawa, Y.; Yagasaki, A. *Inorg. Chem. Commun.* **2008**, *11*, 1267−1269. (b) Maksimovskaya, R. I.; Chumachenko, N. N. *Polyhedron* **1987**, *6*, 1813−1821.
(14) Lee, U.; Joo, H.-C.; Park, K.-M.; Mal, S. S.; Kortz, U.; Keita, B.; Nadjo, L. *Angew. Chem., Int. Ed.* **2008**, *47*, 793−796.
(15) Arumuganathan, T.; Das, S. K. *Inorg. Chem.* **2009**, *48*, 496−507.
(16) Hayashi, Y.; Shinguchi, T.; Kurata, T.; Isobe, K. *ACS Symp. Ser.* **2007**, *974*, 408−423.
(17) (a) Day, V. W.; Klemperer, W. G.; Yagasaki, A. *Chem. Lett.* **1990**, *19*, 1267−1270. (b) Akashi, H.; Isobe, K.; Ozawa, Y.; Yagasaki, A. *J. Cluster Sci.* **1991**, *2*, 291−296. (c) Attanasio, D.; Bachechi, F.; Suber, L. *J. Chem. Soc., Dalton Trans.* **1993**, *15*, 2373−2378. (d) Abe, M.; Isobe, K.; Kida, K.; Nagasawa, A.; Yagasaki, A. *J. Cluster Sci.* **1996**, *7*, 103−107. (e) Hayashi, Y.; Miyakoshi, N.; Shinguchi, T.; Uehara, A. *Chem. Lett.* **2000**, *29*, 170−171.
(18) (a) Paredes-García, V.; Gaune, S.; Saldías, M.; Garland, M. T.; Baggio, R.; Vega, A.; Salah, M.; Fallah, E.; Escuer, A.; Le Fur, E.; Venegas-Yazigi, D.; Spodine, E. *Inorg. Chem. Acta* **2008**, *361*, 3681−3689. (b) Kurata, T.; Hayashi, Y.; Isobe, K. *Chem. Lett.* **2009**, *38*, 218−219.
(19) (a) Heitner-Wirguin, C.; Selbin, J. *J. Inorg. Nucl. Chem.* **1968**, *30*, 3181−3188. (b) Bino, A.; Cohen, S.; Heitner-Wirguin, C. *Inorg. Chem.* **1982**, *21*, 429−431. (c) Baxter, S. M.; Wolczanski, P. T. *Inorg. Chem.* **1989**, *28*, 3263−3264.
(20) Kurata, T.; Uehara, A.; Hayashi, Y.; Isobe, K. *Inorg. Chem.* **2005**, *44*, 2524−2530.
(21) Pecoraro, V. L.; Stemmler, J.; Gibney, B. R.; Bodwin, J. J.; Wang, H.; Kampf, J. W.; Barwinski, A. *Prog. Inorg. Chem.* **1997**, *45*, 83−177.
(22) Khan, M. I.; Tabussum, S.; Doedens, R. J.; Golub, V. O.; O'Connor, C. J. *Inorg. Chem.* **2004**, *43*, 5850−5859.
(23) Ng, C. H.; Lim, C. W.; Teoh, S. G.; Fun, H.-K.; Usman, A.; Ng, S. W. *Inorg. Chem.* **2002**, *41*, 2−3.
(24) (a) Inami, S.; Nishio, M.; Hayashi, Y.; Isobe, K.; Kameda, H.; Shimoda, T. *Eur. J. Inorg. Chem.* **2009**, *34*, 5253−5258. (b) Hayashi, Y. *Coord. Chem. Rev.* **2011**, *255*, 2270−2280.
(25) Day, V. W.; Klemperer, W. G.; Yagasaki, A. *Chem. Lett.* **1990**, 1267−1270.
(26) Kawanami, N.; Ozeki, T.; Yagasaki, A. *J. Am. Chem. Soc.* **2000**, *122*, 1239−1240.
(27) Sheldrick, G. M. *SHELXS-97*; University of Goettingen, Goettingen, Germany, 1997.
(28) Sheldrick, G. M. *SHELXL-97*; University of Goettingen: Goettingen, Germany, 1997.
(29) *teXsan: Crystal Structure Analysis Package*; Molecular Structure Corp.: The Woodlands, TX, 1985 and 1999.
(30) (a) Spek, A. L. *PLATON, A Multipurpose Crystallographic Tool*; Utrecht University: Utrecht, The Netherlands, 2009; (b) Spek, A. L. *Acta Crystallogr.* **2009**, *D56*, 148−155.
(31) Ozutsumi, K.; Handa, K. *Rev. Sci. Instrum.* **2004**, *75*, 111−118.
(32) Taguchi, T.; Ozawa, T.; Yashiro, H. *Phys. Scr.* **2005**, *T115*, 205−206.
(33) Ravel, B.; Newville, M. *J. Synchrotron Radiat.* **2005**, *12*, 537−541.
(34) Newville, M.; Ravel, B.; Haskel, D.; Rehr, J. J.; Stern, E. A.; Yacoby, Y. *Physica B* **1995**, *208/209*, 154−156.
(35) Zabinsky, S. I.; Rehr, J. J.; Ankudinov, A.; Albers, R. C.; Eller, M. *J. Phys. Rev. B* **1995**, *52*, 2995−3009.
(36) Crystallographic data for **3**: $P2_1/c$, a = 23.781(2) Å, b = 44.112(4) Å, c = 25.328(2) Å, β = 95.322(2)°, V = 26455(4) Å^3, Z = 12.
Crystallographic data for **4**: $P2_1/c$, a = 23.959(3) Å, b = 44.038(5) Å, c = 25.239(3) Å, β = 95.464(1)°, V = 26287(5) Å^3, Z = 12.
(37) Chaboy, J.; Marcelli, A.; Tyson, T. A. *Phys. Rev. B* **1994**, *49*, 652−660.
(38) Shannon, R. D. *Acta Crystallogr., Sect. A* **1976**, *32*, 751−767.